Controlled synthesis and photocatalytic performance of ZnO nano/microstructures via facile aqueous solution route

Wenlong Zhang, Yangang Sun

College of Chemistry and Chemical Engineering, Shanghai University of Engineering Science, Shanghai 201620, People's Republic of China
E-mail: syg021@sues.edu.cn

Published in Micro & Nano Letters; Received on 9th July 2013; Revised on 1st August 2013; Accepted on 6th August 2013

Nanosheet-assembled ZnO flower-like ensembles, urchin-like ZnO nanorod assemblies and ZnO nanorods, were synthesised by a facile solution-based route. The Zn^{2+}:OH^- molar ratio was adjusted to obtain ZnO with different morphologies. Scanning electron microscopy, X-ray diffraction and an ultraviolet spectrophotometer were used to observe the morphology, crystal structure and photocatalytic activity of obtained ZnO in detail. The flower-like ZnO ensembles composed of ultra-thin nanosheets exhibited a much better photocatalytic activity than ZnO in the other morphologies, and the decomposition efficiency was 90.26%. It can be concluded that the presence of the photocatalytic activity depends on the morphology of the ZnO samples.

1. Introduction: The facile synthesis of nanostructures with controllable morphology and structure is vital in that the morphology and structure have a profound influence on the properties of nanomaterials and the structural properties can be effectively tuned by tailoring the shape and dimensionality of the nanostructures [1–3]. In the past few years, various nanomaterials with different morphologies have been realised [4–6]. Among them, one-dimensional (1D) nanostructures have been well known for their characteristics of high available specific surface [7] and relatively high electron mobility [8]. In addition, 2D nanomaterials have been reported to have numerous unexpected properties due largely to the unique structural features, such as electrons with a linear dispersion relation [9], ultra-thin thicknesses and possibly exposed specific crystalline planes, which may prove advantageous for a broad range of charge transport involved and surface interaction/reaction oriented applications [10, 11]. Most recently, special attention has been paid to self-assembled 3D superstructures composed of 1D and 2D nanoscale building blocks [12] because such a 3D superstructure combining micro and nanoscaled structures may exhibit some novel or improved physical and chemical properties [13], as well as prevent the aggregation of nanomaterials [14]. Therefore the controllable design of nanostructures with various textures is the focus of the current research [15].

In the field of photocatalysis, the morphologies of photocatalysts deciding the surface-to-volume ratio and affecting surface atomic arrangements and coordination can play an important role in determining catalytic properties, since a photocatalytic reaction mainly occurs at the interface between the catalyst surfaces and organic pollutants [16]. As one of the most important semiconductor photocatalysts, ZnO with different morphologies has attracted considerable interest, because its photocatalytic activity is strongly dependent on the growth behaviour and morphology of the crystal, and different nanostructural ZnO semiconductor materials could result in optimisation of their photocatalytic activity [17].

Significant progress has been made in the preparation of various micro/nanostructured ZnO with rich morphologies [18–20]. Bae *et al.* [21] have used the thermal chemical vapour deposition method to grow ZnO nanorods (80–150 nm in diameter and 3 μm in length) on a prefabricated 1D nanostructure such as carbon nanotube, GaP, GaN and SiC nanowires. Dong *et al.* [22] reported the synthesis of single-crystalline mesoporous ZnO nanomaterials which were ultra-thin with a thickness of about 10 nm, through a green anti-solvent process followed by calcination at 300°C, and explored their photocatalytic properties. By sonicating an aqueous solution of zinc acetate dehydrate and ammonia–water at room temperature using a frequency of 20 kHz and an intensity of 39.5 W cm^2 for 30 min, nanorods-assembled ZnO microflowers with an average diameter of 1.5 μm have been synthesised and nanorods that constituted individual petals on the flowers were found to have sharp ends [23]. However, the complicated procedures, sophisticated equipment or rigid experimental conditions used in these methods severely restrict their large-scale application for industry. Furthermore, despite this recent progress, there are still some difficulties in the shape-controlled synthesis of ZnO nanocrystals, especially regarding control over the complex structure. Hence, from the technological point of view, it is strongly desirable to develop more convenient, economical, template-free techniques to answer the demand for exploring the photocatalytic property of ZnO materials.

In this Letter, we provide a simple solution-based route for synthesising ZnO with well-defined morphologies including flower-like ensembles composed of ultra-thin nanosheets, urchin-like nanorod assemblies and monodisperse nanorods under mild conditions by simply regulating the molar ratio of Zn^{2+} to OH^- with excellent reproducibility. The different morphologies of ZnO nano or microstructures were investigated by scanning electron microscope (SEM) images, and we also explored the photocatalytic activities of ZnO with different morphologies by photodegradation of dye methyl orange (MO).

2. Experimental: All the reagents were analytically pure and used without further purification. In a typical procedure, according to the molar ratio of Zn^{2+}:OH^-, some amount of NaOH (4 mol/l) was added dropwise into 10 ml of 1 mol/l $Zn(NO_3)_2 \cdot 6H_2O$ aqueous solution with 2.5 ml of sodium dodecyl sulphate (SDS, 0.2 mol/l) and a certain volume of distilled water under strong magnetic stirring at 3°C to obtain a 50 ml clear solution. The solution was then kept at room temperature for 1.5 h under vigorous stirring to obtain the precursor and subsequently transferred to a ground-glass stopped conical flask, ageing at 85°C for 5 h. The white products deposited on the bottom of the conical flask were collected, washed with distilled water to remove residual reactants and dried at ambient temperature. The products were characterised with an X-ray diffractometer (XRD; Rigaku D/Max-2550 PC) equipped with Cu Kα radiation and SEM (JSM-5600LV).

A top-irradiation reactor was used as the photoreactor. Each photoreactor contained 100 ml dye aqueous solution (MO, 10.0 mg/l) and 80 mg of as-obtained ZnO with different morphologies served as photocatalysts. The reaction system was stirred for 60 min to reach the adsorption equilibrium of the dye. Irradiation was performed with a xenon lamp (Model PLS-SXE300). The top-irradiation reactor was placed about 10 cm below the light source, and irradiated for different periods at room temperature under magnetic stirring. The efficiency of the degradation processes was analysed by monitoring the intensity of the absorption peak at the maximum absorption wavelength, using a UV/vis spectrometer (Perkin Elmer, Lambda 35). After a given irradiation time, the aqueous suspension of about 3.5 ml was taken from the reactor, centrifuged and the absorbance of the clear solution was measured on a PerkinElmer to determine the contents of MO.

3. Results and discussion: Fig. 1*a* presents the typical XRD patterns of the samples synthesised with different Zn^{2+}:OH^{-} molar ratios. All the peaks of each sample can be indexed to a hexagonal ZnO phase with lattice constants of $a = 0.325$ nm and $c = 0.521$ nm (JCPDS Card No. 36-1451). No characteristic peaks from precursor impurities, such as $Zn(NO_3)_2{\cdot}6H_2O$ and SDS, are detected within the experimental error. According to the intensity and half width of the XRD patterns, even if fabricated at low temperature, these ZnO nanoparticles crystallised well.

It should be noted that the three samples exhibited different relative intensities of (100) to (002) peaks ($I_{(100)}/I_{(002)}$) reflecting the preferential crystallographic orientation of the prepared ZnO products. As shown in Fig. 1*b*, the intensity ratio of (100)/(002) evidently increases with increasing of the molar ratio of Zn^{2+}:OH^{-}. It is found to be 0.99 for sample a, and to increase to 1.10 and 1.31 for samples b and c, respectively.

The corresponding morphologies and detailed structures were characterised by SEM examinations, as shown in Fig. 2. Figs. 2*a* and *b* show the SEM image of the products synthesised with Zn^{2+}:OH^{-} molar ratio to 1:2.4 (sample a). The products look like dense flowers assembled from varying amounts of very small ultra-thin nanosheets as illustrated in Fig. 2*a*. The magnified SEM image (Fig. 2*b*) reveals that the products are 3D porous flowers. The SEM images also confirm the ultra-thin nanostructures of the products with a typical thickness of ~20–30 nm and the other two dimensions reach ~500–2000 nm, which is in good agreement with the XRD. Furthermore, the interconnected small nanosheets create abundant space, which ensures an easier molecule transport and more superficial photocatalytic species. When the molar ratio of Zn^{2+}:OH^{-} is increased to 1:4, the ZnO products exhibit uniform urchin-like ZnO structures consisting of hexagonal cones with ~200 nm diameter and ~1.2μm length (sample b), as can be seen in Figs. 2*c* and *d*. With further increase of the Zn^{2+}:OH^{-} molar ratio to 1:4.8, highly monodisperse ZnO nanorods with sharp tips (sample c) were obtained with diameter and length of about 200 nm and 2 μm, respectively (Figs. 2*e* and *f*).

To evaluate the photocatalytic activities of the ZnO samples, the photocatalytic properties of as-synthesised ZnO with different morphologies were studied employing the degradation of the solution of dye MO. The measurement of absorption intensity is given at various intervals for the intensity of the characteristic absorption peak of MO at 464 nm with significant changing. Fig. 3*a* shows different variations in the UV–vis absorption spectra of MO using the nanosheet-assembled ZnO flower-like ensembles as catalyst at different time intervals under xenon lamp illumination. It can be clearly seen from Fig. 3*a* that the main absorption is at 464 nm, the absorbance value decreased rapidly at the maximum absorption peak location (464 nm) of MO with the extension of the irradiation time of the light and the intensity of the absorption peak at 464 nm was 0.0686 after 3.0 h irradiation under the xenon lamp, suggesting that the ZnO flower-like ensembles behaved as an effective catalyst for photodegrading MO. To explore further the morphology induced changing of the photocatalytic activities for as-obtained ZnO samples, the degradation reactions for the urchin-like ZnO nanorod assemblies and the ZnO nanorods were also investigated

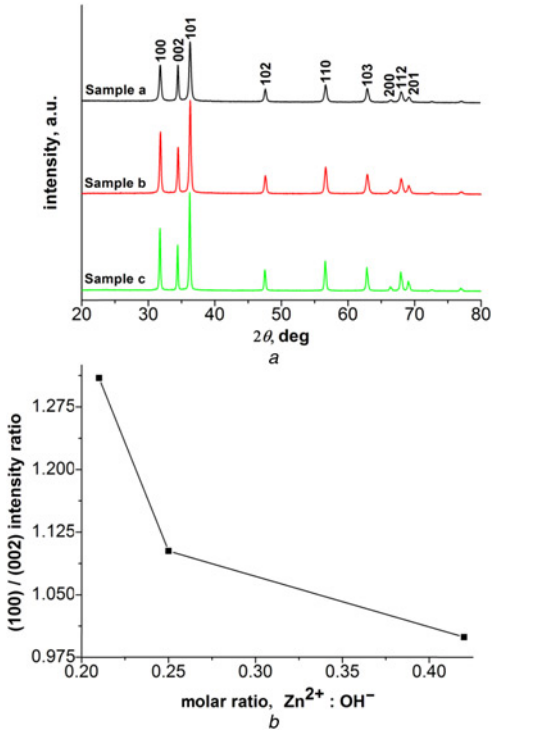

Figure 1 *XRD patterns of products prepared corresponding to different Zn^{2+}:OH^{-} molar ratios, sample a 1:2.4, sample b 1:4, sample c 1:4.8; and plot of (100)/(002) intensity ratio against Zn^{2+}:OH^{-} molar ratios*
a XRD patterns
b Plot of (100)/(002) intensity ratio against Zn^{2+}:OH^{-} molar ratios

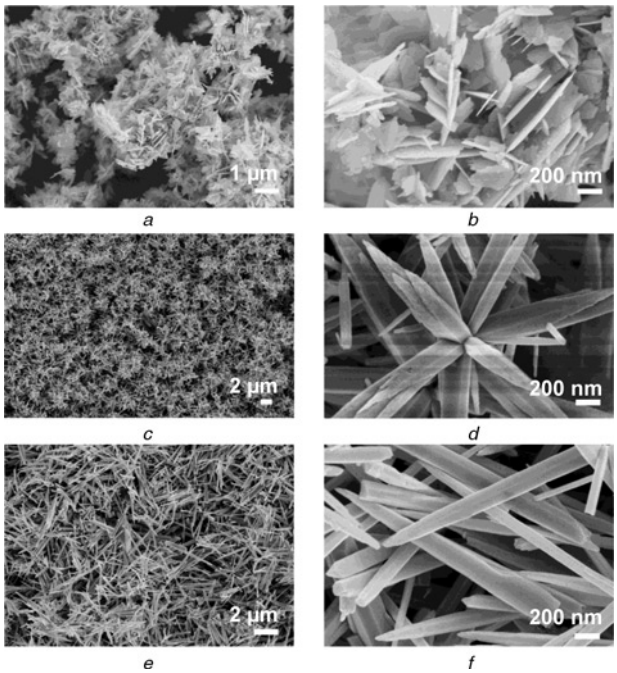

Figure 2 *Characterisation of ZnO nano/microstructures*
a and *b* SEM image of ZnO flower-like ensembles
c and *d* SEM image of ZnO urchin-like assemblies
e and *f* SEM image of ZnO nanorods

doi: 10.1049/mnl.2013.0425

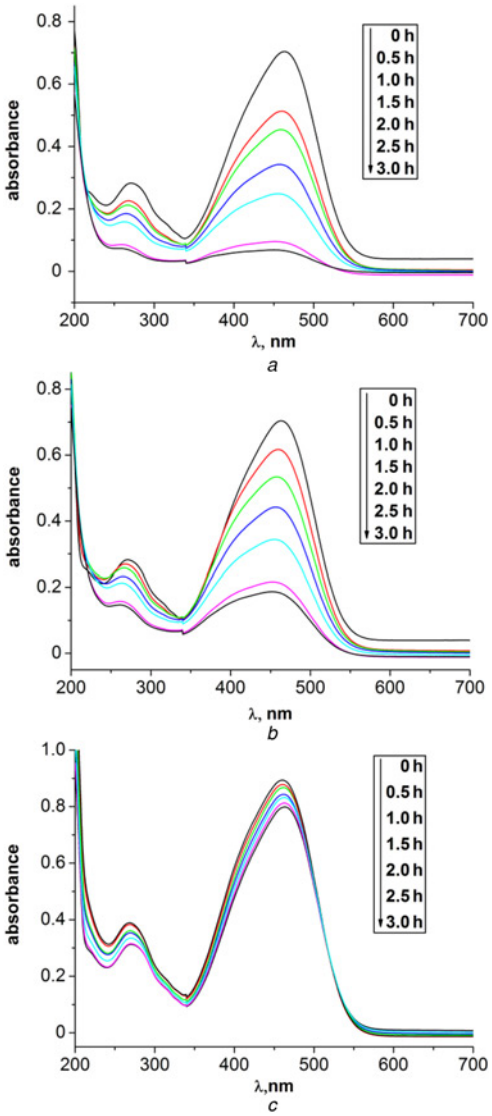

Figure 3 *Time dependent UV–vis spectral changes of MO aqueous solution under xenon lamp irradiation*
a Spectral changes of MO solutions upon photodegradation catalysed by ZnO flower-like ensembles
b Spectral changes of MO solutions upon photodegradation catalysed by ZnO urchin-like assemblies
c Spectral changes of MO solutions upon photodegradation catalysed by ZnO nanorods

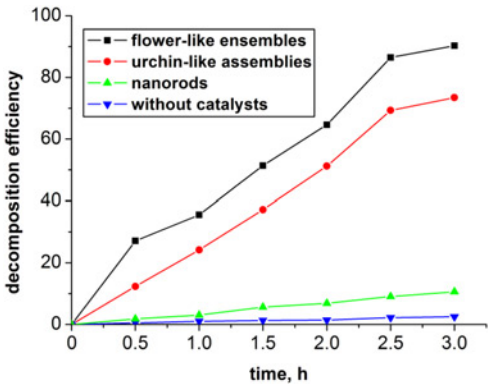

Figure 4 *Decomposition efficiency of MO catalysed by ZnO flower-like ensembles, ZnO urchin-like assemblies, ZnO nanorods, as well as only induced by irradiation*

under the same experimental conditions, and the intensities of the absorption peak at 464 nm were 0.1869 and 0.7996, respectively, after 3.0 h illumination (see Figs. 3*b* and *c*), distinctly higher than that of the nanosheet-assembled ZnO flower-like ensembles. This clearly demonstrates that the ZnO flower-like ensembles have better activity than the other ZnO morphologies, whereas the ZnO nanorods exhibited the least photocatalytic performance.

According to the Beer-Lambert law, the concentration of MO is approximately linearly proportional to the intensity of the absorption peak at 464 nm [24], which is at the maximum of the full absorption band. The decomposition efficiency of MO can be calculated by using the following formula, MO decomposition (%) = $100 \times (C_0–C)/C_0$, where C_0 and C are the equilibrium concentrations of MO before and after irradiation, respectively.

The decomposition efficiency of MO over the ZnO samples varied with the irradiation time in Fig. 4. It can be observed that several processes in the presence of catalysts were obviously photo-driven reactions compared with the procedure without catalysts, revealing that ZnO active material as photocatalysts can play a very important role in photo-driven reactions. The nanosheet-assembled flower-like ensembles showed the highest photocatalytic activity (90.26%), followed by urchin-like nanorod assemblies (73.45%), and nanorods (10.62%). It is obvious that the photocatalytic efficiency was greatly improved with the conversion of ZnO nanostructures from nanorods to the urchin-like nanorod assemblies, especially the nanosheet-assembled flower-like ensembles. This finding is exciting for the exploration of photocatalysts with high efficiency.

As to the origins of the photocatalytic superiority of the nanosheet-assembled ZnO flower-like ensembles, two possible reasons should be noted. Firstly, the ultra-thin ZnO nanosheets cause the enhanced dye-adsorption and light-harvesting owing to the larger specific surface area [25]. Also, the ultra-thin sheet-like structures could enhance the efficiency of the electron–hole separation. This is for the reason that nanosheets with ultra-thin thickness will benefit from the transfer of the photo-generated charge carriers from the inside to the surface of the crystal where they react with the MO molecules [26, 27]. In addition, the ultra-thin thickness of the nanosheets is ~20–30 nm, which is very close to the regime where quantum size effect is prominent. The nanosheets of different sizes would promote charge transfer in the materials, and the increase in the charge-transfer rates dramatically reduces direct recombination of the light-generated electron–hole pairs [28]. Secondly, the disordered arrangement of nanosheets in the flower-like 3D ZnO ensembles can effectively prevent aggregation and thus maintain a large active surface area. The large active surface area and capacious interspaces of the flower-like porous structure offer more opportunity for the diffusion and mass transportation of MO molecules and hydroxyl radicals in the photochemical reaction of MO degradation [27, 29]. Furthermore, ZnO flower-like structures are easy to be separate from solutions because of their large size, and this material still maintained 92.1% of the photocatalytic activity after three cycles. All these indicated that the ZnO flower-like structures could serve as a good candidate for the degradation of organic pollutants.

4. Conclusions: In summary, ZnO with well-defined morphologies have been prepared by a simple aqueous solution route at low temperature. The morphology of ZnO greatly changed from nanosheet-assembled flower-like ensembles, urchin-like nanorod assemblies to nanorods with increasing of the Zn^{2+}:OH^- molar ratio. The photocatalytic efficiency was greatly improved with the conversion of ZnO nanostructures from nanorods to the urchin-like nanorod assemblies, especially the flower-like ensembles composed of ultra-thin nanosheets. This Letter not only provides a low-cost and amendable to large-scale production method for the preparation of ZnO with various morphologies in

design, but also increases its photocatalytic degradation efficiency in organic pollutant treatment.

5. Acknowledgments: This research was supported by the Foundation of Shanghai University of Engineering Science, China (grant number 2012gp13), and the Open Fund of the State Key Laboratory for the Modification of Chemical Fibers and Polymer Materials, Dong Hua University (grant number LK1209).

6 References

[1] Zeng H.C.: 'Synthesis and self-assembly of complex hollow materials', *J. Mater. Chem.*, 2011, **21**, pp. 7511–7526

[2] Nam K.T., Kim D.W., Yoo P.J., *ET AL.*: 'Virus-enabled synthesis and assembly of nanowires for lithium ion battery electrodes', *Science*, 2006, **312**, pp. 885–888

[3] Na J.S., Gong B., Scarel G., Parsons G.N.: 'Surface polarity shielding and hierarchical ZnO nano-architectures produced using sequential hydrothermal crystal synthesis and thin film atomic layer deposition', *ACS Nano*, 2009, **3**, pp. 3191–3199

[4] Sun Y.G., Xia Y.N.: 'Resonance in large noble metal clustes', *Science*, 2002, **298**, pp. 2176–2179

[5] Zhang P., Gao L.: 'Wet chemical synthesis of ultralong and straight single-crystalline ZnO nanowires and their excellent UV emission properties', *J. Mater. Chem.*, 2003, **13**, pp. 2551–2554

[6] Tang C.C., Bando Y., Golberg D., Ma R.: 'Cerium phosphate nanotubes: synthesis, valence state, and optical properties', *Angew. Chem., Int. Ed.*, 2005, **44**, pp. 576–579

[7] Li C., Qi L.M.: 'Colloidal-crystal-assisted patterning of crystalline materials', *Adv. Mater.*, 2010, **22**, pp. 1494–1497

[8] Schmidt-Mende L., MacManus-Driscoll J.L.: 'ZnO-nanostructures, defects and devices', *Mater. Today*, 2007, **10**, pp. 40–48

[9] Kim K.S., Zhao Y., Jang H., *ET AL.*: 'Large-scale pattern growth of graphene films for stretchable transparent electrodes', *Nature*, 2009, **457**, pp. 706–710

[10] Qiu Y.C., Chen W., Yang S.H.: 'Facile hydrothermal preparation of hierarchically assembled, porous single-crystalline ZnO nanoplates and their application in dye-sensitized solar cells', *J. Mater. Chem.*, 2010, **20**, pp. 1001–1006

[11] Jing Z.H., Zhan J.H.: 'Fabrication and gas-sensing properties of porous ZnO nanoplates', *Adv. Mater.*, 2008, **20**, pp. 4547–4551

[12] Li J., Fan H.Q., Jia X.H.: 'Multi layered ZnO nanosheets with 3D porous architectures: synthesis and gas sensing application', *J. Phys. Chem. C*, 2010, **114**, pp. 14684–14691

[13] Innocenzi P., Malfatti L., Soler-Illia G.J.A.A.: 'Hierarchical mesoporous films: from self-assembly to porosity with different length scales', *Chem. Mater.*, 2011, **23**, pp. 2501–2509

[14] Polshettiwar V., Baruwati B., Varma R.S.: 'Self-assembly of metal oxides into three-dimensional nanostructures: synthesis and application in catalysis', *ACS Nano*, 2009, **3**, pp. 728–736

[15] Liu S.W., Li C., Yu J.G., Xiang Q.J.: 'Improved visible-light photocatalytic activity of porous carbon self-doped ZnO nanosheet-assembled flowers', *Cryst. Eng. Commun.*, 2011, **13**, pp. 2533–2541

[16] Lu H.B., Wang S.M., Zhao L., Li J.C., Dong B.H., Xu Z.X.: 'Hierarchical ZnO microarchitectures assembled by ultrathin nanosheets: hydrothermal synthesis and enhanced photocatalytic activity', *J. Mater. Chem.*, 2011, **21**, pp. 4228–4234

[17] Das J., Khushalani D.: 'Nonhydrolytic route for synthesis of ZnO and its use as a recyclable photocatalyst', *J. Phys. Chem. C*, 2010, **114**, pp. 2544–2550

[18] Sounart T.L., Liu J., Voigt J.A., Huo M., Spoerke E.D., McKenzie B.: 'Secondary nucleation and growth of ZnO', *J. Am. Chem. Soc.*, 2007, **129**, pp. 15786–15793

[19] Sun Y.G., Hu J.Q., Wang N., *ET AL.*: 'Controllable hydrothermal synthesis, growth mechanism, and properties of ZnO three-dimensional structures', *New J. Chem.*, 2010, **34**, pp. 732–737

[20] Yu L.M., Fan X.H., Cao L., Shui J.Y., Yan W.: 'Shape-controlled cluster growth of ZnO nanoflowers using sol–gel method', *Micro Nano Lett.*, 2012, **7**, pp. 1046–1048

[21] Bae S.Y., Seo H.W., Choi H.C., Park J.: 'Heterostructures of ZnO nanorods with various one-dimensional nanostructures', *J. Phys. Chem. B*, 2004, **108**, pp. 12318–12326

[22] Dong J.Y., Lin C.H., Hsu Y.J., Lu S.Y., Wong D.S.H.: 'Single-crystalline mesoporous ZnO nanosheets prepared with a green antisolvent method exhibiting excellent photocatalytic efficiencies', *Cryst. Eng. Commun.*, 2012, **14**, pp. 4732–4737

[23] Jung S.-H., Oh E., Lee K.-H., *ET AL.*: 'Sonochemical preparation of shape-selective ZnO nanostructures', *Cryst. Growth Des.*, 2008, **8**, pp. 265–269

[24] Wang X.J., Pang Z.W., Wu M.Z., *ET AL.*: 'Simple hydrothermal route to synthesise a nanocrystalline ZnO/PVP composite film and its optical property', *Micro Nano Lett.*, 2012, **7**, pp. 523–525

[25] Lu H.B., Wang S.M., Zhao L., Li J.C., Dong B.H., Xu Z.X.: 'Hierarchical ZnO microarchitectures assembled by ultrathin nanosheets: hydrothermal synthesis and enhanced photocatalytic activity', *J. Mater. Chem.*, 2011, **21**, pp. 4228–4234

[26] Zhang L.Z., Yu J.C.: 'A sonochemical approach to hierarchical porous titania spheres with enhanced photocatalytic activity', *Chem. Commun.*, 2003, **16**, pp. 2078–2079

[27] Wang X.C., Yu J.C., Ho C.M., Hou Y.D., Fu X.Z.: 'Photocatalytic activity of a hierarchically macro/mesoporous titania', *Langmuir*, 2005, **21**, pp. 2552–2559

[28] Ye C.H., Bando Y., Shen G.Z., Golberg D.: 'Thickness-dependent photocatalytic performance of ZnO nanoplatelets', *J. Phys. Chem. B*, 2006, **110**, pp. 15146–15151

[29] Sun H.Y., Yu Y.L., Luo J., Ahmad M., Zhu J.: 'Morphology-controlled synthesis of ZnO 3D hierarchical structures and their photocatalytic performance', *Cryst. Eng. Commun.*, 2012, **14**, pp. 8626–8632

doi: 10.1049/mnl.2013.0425